Published in final edited form as:
J Am Chem Soc. 2015 May 6; 137(17): 5793–5797. doi:10.1021/jacs.5b01520.

Single-molecule analyte recognition with ClyA nanopores equipped with internal protein adaptors

Misha Soskine[#1,2], **Annemie Biesemans**[#2], and **Giovanni Maglia**[1,2,*]

[1]Groningen Biomolecular Sciences & Biotechnology (GBB) Institute, University of Groningen, 9747 AG, Groningen, The Netherlands [2]Department of Chemistry, University of Leuven, Leuven, 3001, Belgium

[#] These authors contributed equally to this work.

Abstract

Nanopores have been used to detect molecules, to sequence DNA or to investigate chemical reactions at the single-molecule level. Because they approach the absolute limit of sensor miniaturisation, nanopores are amenable to parallelisation and could be used in single-cell measurements. Here we show that single enzymes can be functionally and reversibly trapped inside the confined space of a ClyA nanopore. Remarkably, the binding of ligands to the internalised proteins is mirrored by specific changes to the nanopore conductance. Conveniently, the manipulation of the charge of the protein allowed increasing of the residence time of the protein inside the nanopore. Nanopores with internalised protein adaptors can be used to study proteins in real-time or can be incorporated into inexpensive portable devices for the detection of analytes with high selectivity.

Introduction

Over the past two decades nanopore analysis has emerged as a promising analytical tool for single-molecule analysis[1-4]. Nanopore technology allows the investigation of native molecules with high sampling bandwidth without the need for labelling, chemical modifications or surface immobilisation. Further, the ionic current output signal can be easily interfaced with miniaturised and portable electronic devices. For instance, arrays of nanopores integrated into a MinION™ sequencer have been recently used for the profiling of genomic DNA[5-7]. Furthermore, biological nanopores have been reconstituted into bilayers formed on glass nanopipettes[8] and on glass tips for scanning ion-conductance

[*]***Corresponding Author***: Giovanni Maglia Giovanni Maglia, PhD, University of Groningen, Groningen Biomolecular Sciences & Biotechnology (GBB) Institute,Nijenborgh 7, 9747 AG, PO Box 11103, 9700 CC, Groningen, The Netherlands, Phone: +31(0)50 363 6138, g.maglia@rug.nl.

ASSOCIATED CONTENT

Supporting Information

Additional text, Materials and methods, Supporting Tables, Supporting Figures. This material is available free of charge via the Internet at http://pubs.acs.org.

The authors declare no competing financial interests.

Europe PMC Funders Author Manuscripts

microscopy[9]. Therefore, nanopore-functionalized nanopipettes that can detect and quantify metabolites are promising platforms for measurement in single cells.

Previous studies showed that small molecules binding to cyclodextrin[10] and cyclic peptide[11] adaptors or cucurbiturils carriers[12] could be detected by ionic current recordings using the α-hemolysin (αHL) nanopore. However, such guest adaptors and carriers do not bind selectively to host molecules, making the identification of analytes in a complex mixture of compounds a real challenge. By contrast, proteins have evolved to identify their ligands with high specificity in a sea of very similar chemical species. Therefore, nanopores equipped with protein adaptors would be ideal elements for integration into nanopore-based sensing devices for the analysis of complex biological samples. However, building such hybrid devices is challenging. Proteins are too large to be incorporated into the αHL and other biological nanopores[13-15] and mostly translocate through solid-state nanopores too fast to be properly sampled [16]. Further, it is not known if the environment of the nanopore lumen is compatible with enzymatic functions, as experiments with solid-state nanopores revealed that proteins might be stretched by the electrical field[17] and unfolded under applied potentials higher than +200 mV[18].

Recently, we showed that folded proteins enter the lumen of Type I ClyA-AS (C87A/L99Q/E103G/F166Y/I203V/C285S/K294R/H307Y), a dodecameric[19] engineered version of ClyA from *Salmonella Typhi* selected for its favourable properties in planar lipid bilayers[20]. Conveniently, ClyA also assembles into higher oligomeric forms (Type II and Type III ClyA)[20] that are large enough to accommodate, for example, protein-DNA complexes [21]. Notably, we showed that electroosmotic and electrophoretic forces allowed trapping proteins such as thrombin inside the ~240 nm^3 cavity of Type I ClyA nanopores for tens of minutes[20,22], suggesting that protein adaptors might be paired to ClyA nanopores without the use of covalent chemistry or other immobilisation techniques. In this work we report that the binding of analytes to two model proteins incorporated inside a ClyA nanopore is reflected by changes in the nanopore conductance, indicating that proteins immobilised inside the nanopore remain functional. Moreover, electrical readouts of nanopore-confined proteins will have applications in the fabrication of sensor arrays for the discovery of new therapeutics or the detection of biomarker analytes in biological samples.

Results and discussion

As a first model protein we selected *E. coli* AlkB demethylase (Mw=25 kDa), a globular protein that is expected to pass the *cis* entry of ClyA, but is too large to traverse the *trans* exit of the nanopore (Figure 1a,b). In complex with iron ions (AlkB-Fe^{++}) AlkB co-oxidises methylated DNA and its cofactor 2-oxoglutarate (2-OG), producing succinate (SUC), carbon dioxide and formaldehyde[23,24]. 2-oxoglutarate is an important metabolite that influences aging and age-related diseases[25], and is a biomarker for non-alcoholic fatty liver disease[26], heart failure[27] and cardiorenal syndrome [27]. The level of succinate in urine is a biomarker for kidney damage [28].

Individual AlkB-Fe^{++} molecules were studied using Type I ClyA-AS (ClyA-AS hereafter). In 150 mM NaCl, 15 mM Tris HCl and pH 8.0 ClyA-AS formed nanopores with a steady

open pore conductance (I_O = −1.7±0.1 nSi, average±SD, N=38, −60 mV, 28°C) under a wide range of applied potentials. Here and hereafter *N* indicates the number of independent single nanopore experiments, n_p the number of individual protein blockades and n_l the total number of ligand binding events analysed. The addition of AlkB-Fe^{++} (~4 nM) to the *cis* side of ClyA-AS provoked current blockades (I_B), quoted here as residual currents calculated as a percentage of the open pore current ($I_{RES\%}$), due to the electroosmotic confinement of AlkB-Fe^{++} between the wider *cis* entrance and the narrower *trans* exit of the protein nanopore (Figure 1b)[20,22]. Conveniently, AlkB-Fe^{++} remained trapped inside the nanopore for several minutes (Figure 1c). The signal induced by AlkB-Fe^{++} fluctuated between two distinctive current levels, L1 ($I_{RES\%}$ = 52.6±2.0%, n_p=15, N=7) and L2 ($I_{RES\%}$ = 39.0±1.0%, n_p=15, N=7, Figure 1c), possibly due to two residence sites for the protein within the lumen of the ClyA-AS nanopore[22].

At −60 mV the addition to the *cis* reservoir of the cofactor (2-OG), an isosteric inhibitor (N-oxalylglycine, N-OG) or the processed cofactor (SUC) induced reversible current enhancements within the AlkB-Fe^{++} blockades ($\Delta I_{RES\%}$= +4.7±1.3%, +4.9±1.0 and +4.6±1.3, respectively, n_p>15, n_l > 75, N>4, Figure 2a, Figure S1,2 and Table S1) that showed a mean duration (τ_{off}) of 1.7±0.5 s, 1.8±0.4 s and 61±11 ms, respectively (n_l>4500, N>8, and n_p>80). The current enhancements were also observed from the current level L2 (Figure S2). We hypothesised that such current events reflected the conformational changes occurring during the transition from the open conformation of the apo-enzyme to the closed state of the ligand-bound form of AlkB-Fe^{++} (Figure 2a)[29,30]. To confirm this hypothesis we tested an AlkB mutant where the asparagine at position 120, which has been reported to be involved in the binding of 2-OG to AlkB[29], was substituted by aspartate (N120D). The addition of 7.2 mM of 2-OG did not induce current transitions to the N120D-AlkB-Fe^{++} blockades (*N*=4, Figure 2a), suggesting that the affinity of this AlkB mutant for 2-OG is strongly reduced. As expected for a protein-ligand association process the dissociation rate constants (k_{off}, Table S2), measured from the inverse of the dwell times of the ligand-binding events ($1/\tau_{off}$), did not depend on the concentration of the ligand, while the frequencies of the ligand-induced events ($f = 1/\tau_{on}$) increased linearly with the concentration of the three ligands, from which slopes the association rate constants (k_{on}) could be calculated (Figure 2b, Table S2).

E. coli dihydrofolate reductase (DHFR, Mw=19 kDa) was selected as a second model protein adaptor (Figure 3a,b). During the DHFR catalytic cycle dihydrofolate is reduced to tetrahydrofolate and the cofactor NADPH is oxidised to NADP+. Tetrahydrofolate is a cofactor in many metabolic reactions, thus inhibitors of DHFR such as methotrexate (MTX) are antibiotic and anticancer agents. The ratio of the NADP+ and NADPH intracellular concentrations is used to monitor the oxidative stress in cells[32]. We found that apo-DHFR, which is smaller than AlkB, dwelled inside ClyA-AS only for a few milliseconds. Upon the addition of MTX to the *cis* solution the frequency and the dwell time of the protein blockades decreased, while the residual current increased (supporting results). The blockades were then abolished by the subsequent addition of NADPH to the same side (Figure S3). Since both the inhibitor and the cofactor are negatively charged, these results suggested that the additional negative charges increased the electrophoretic/electrostatic

drag force opposing DHFR entry and residence inside the nanopore. In order to increase the residence time of the protein, we engineered DHFR by introducing a polypeptide tag containing four additional positive charges at the C-terminus of the protein ($DHFR_{tag}$, supporting results, Figure S4). In complex with MTX, $DHFR_{tag}$, added to the *cis* compartment, induced current blockades with a mean dwell of 3.1±1.4 s (*N*=5, n_p=230, Figure 3c) that was three orders of magnitude longer than $DHFR_{tag}$ or DHFR:MTX blockades mean dwell times. A possible explanation to this result is that, tuned by the additional positive charges, the binary $DHFR_{tag}$:MTX complex is at a potential minimum inside the nanopore where the electroosmotic, electrophoretic and electrostatic forces are balanced. The dissociation of MTX from the binary complex was slower than the residence time of the complex inside the nanopore and could not be observed by ionic current recordings. As shown before with apo-AlkB-Fe^{++}, $DHFR_{tag}$:MTX blockades showed a main current level L1 ($L1_M$, $I_{RES\%}$ = 74.7±0.5%, n_p =25, *N*=5) that rarely visited a second current level L2 ($L2_M$, $I_{RES\%,}$ = 53.5±0.9%, n_p =25, N=5, Figure 3c).

At −90 mV the addition of the oxidised cofactor NADP+ to the *trans* compartment of ClyA-AS produced reversible current enhancements to the $DHFR_{tag}$:MTX complex blockades formed in the *cis* solution ($L1_{M:N+}$, $\Delta I_{RES\%}$= +2.3±0.5%, n_p =15 blockades, n_l > 225, *N*=3; and $\tau_{M:N+}$ = 102±11 ms, n_l =19,000, N=9 n_p > 800, Figure 4a, Table S3, Figure S5). Association and dissociation rate constants could be measured from titration experiments (Figure 4b, Table S4). NADPH added to the *trans* compartment also induced additional current enhancements to the binary complex blockades (Figure 4a). Remarkably, the current events induced by NADPH showed a slightly higher residual current ($L1_{M:NH}$, $\Delta I_{RES\%}$= +2.7±0.7%, n_p =15 n_l=15, *N*=4 Table S3) than the NADP+ blockades ($\Delta I_{RES\%}$= +2.3±0.5%) and had a dwell time longer than the residence time of the ternary complex inside the nanopore (Figure 4a). As a consequence, despite the minute difference between NADPH and NADP+ (a hydride ion), the binding of the two ligands to $DHFR_{tag}$:MTX could be clearly differentiated (Figure 4a).

Although the bulk kinetic constants for the binding of NADP+ and NADPH to MTX:DHFR could not be retrieved from the literature, the equilibrium dissociation constant for the binding of 2-OG to AlkB-Mn^{++} was recently measured by an intrinsic tryptophan fluorescence quenching assay (K_D^{bulk}= 4.1±0.6 10^{-6} M at 24 °C)[31]. By comparison, the equilibrium dissociation constant of 2-OG for AlkB-Fe^{++} inside the nanopore measured from the ratio of the association and dissociation constants (K_D^{pore} =k_{off}/k_{on}) was about two orders of magnitude higher than the bulk value (K_D^{pore}=3.7±1.9 10^{-4} M, −60 mV, 28°C). This effect is likely to be related to the confinement of AlkB-Fe^{++} inside the nanopore and to the effect of the applied potential. ClyA nanopores have a negatively charged interior and are, therefore, cation selective.[33] Thus, under negative applied potentials (*trans*) the diffusion of the negatively charged ligands added to the *cis* solution through the nanopore is likely to be opposed. This is probably to be further accentuated by the unfavourable electrostatic interaction between the ligands and the wall of the nanopore lumen. This complication might be overcome by using nanopores with an internal charge with an opposite sign to that of the ligand to detect.

Conclusions

The results presented here indicate that the binding of analytes to proteins trapped inside ClyA can be monitored by specific changes in the nanopore conductance, suggesting that proteins confined inside nanopores remain functional. Proteins with suitable size and shape, such as AlkB, are sterically trapped between the wider *cis* entrance and the narrower *trans* exit of the pore. Smaller proteins, such as DHFR, that escape ClyA too quickly to allow the sampling of ligand binding kinetics, can be engineered with genetically encoded extensions to increase their residence time inside the nanopore. Our approach should also be applicable to larger protein adaptors, which could be internalised into larger nanopores such as higher oligomeric forms of ClyA [20], Phi29 [34], pneumolysin [35] or solid-state nanopores. Since most biologically active molecules have a protein target, nanopores with an internal protein adaptor are promising systems for integration in miniaturised low-cost electronic devices for medical, forensics or environmental monitoring or for single-cell analysis.

Supplementary Material

Refer to Web version on PubMed Central for supplementary material.

ACKNOWLEDGMENT

We thank the European Research Council (European Commission's Seventh Framework Programme, project n° 260884) for funding. AB is funded by a Ph.D. grant from the Agency for Innovation by Science and Technology (IWT) Flanders.

REFERENCES

(1). Howorka S, Siwy Z. Chemical Society Reviews. 2009; 38:2360. [PubMed: 19623355]
(2). Bayley H. Clinical chemistry. 2015; 61:25. [PubMed: 25477535]
(3). Luchian T, Shin SH, Bayley H. Angewandte Chemie-International Edition. 2003; 42:3766.
(4). Bezrukov SM, Vodyanoy I, Parsegian VA. Nature. 1994; 370:279. [PubMed: 7518571]
(5). Ashton PM, Nair S, Dallman T, Rubino S, Rabsch W, Mwaigwisya S, Wain J, O'Grady J. Nature biotechnology. 2014
(6). Mikheyev AS, Tin MM. Molecular ecology resources. 2014; 14:1097. [PubMed: 25187008]
(7). Quick J, Quinlan AR, Loman NJ. GigaScience. 2014; 3:22. [PubMed: 25386338]
(8). White RJ, Ervin EN, Yang T, Chen X, Daniel S, Cremer PS, White HS. J Am Chem Soc. 2007; 129:11766. [PubMed: 17784758]
(9). Zhou Y, Bright LK, Shi W, Aspinwall CA, Baker LA. Langmuir. 2014; 30:15351. [PubMed: 25425190]
(10). Gu LQ, Braha O, Conlan S, Cheley S, Bayley H. Nature. 1999; 398:686. [PubMed: 10227291]
(11). Sanchez-Quesada J, Ghadiri MR, Bayley H, Braha O. Journal of the American Chemical Society. 2000; 122:11757.
(12). Braha O, Webb J, Gu LQ, Kim K, Bayley H. Chemphyschem. 2005; 6:889. [PubMed: 15884071]
(13). Jung Y, Cheley S, Braha O, Bayley H. Biochemistry. 2005; 44:8919. [PubMed: 15966717]
(14). Movileanu L, Howorka S, Braha O, Bayley H. Nature Biotechnology. 2000; 18:1091.
(15). Fahie M, Chisholm C, Chen M. ACS nano. 2015; 9:1089. [PubMed: 25575121]
(16). Plesa C, Kowalczyk SW, Zinsmeester R, Grosberg AY, Rabin Y, Dekker C. Nano Letters. 2013; 13:658. [PubMed: 23343345]
(17). Oukhaled A, Cressiot B, Bacri L, Pastoriza-Gallego M, Betton JM, Bourhis E, Jede R, Gierak J, Auvray L, Pelta J. ACS nano. 2011; 5:3628. [PubMed: 21476590]

(18). Freedman KJ, Haq SR, Edel JB, Jemth P, Kim MJ. Sci Rep. 2013; 3:1638. [PubMed: 23572157]
(19). Mueller M, Grauschopf U, Maier T, Glockshuber R, Ban N. Nature. 2009; 459:726. [PubMed: 19421192]
(20). Soskine M, Biesemans A, De Maeyer M, Maglia G. J Am Chem Soc. 2013; 135:13456. [PubMed: 23919630]
(21). Van Meervelt V, Soskine M, Maglia G. ACS nano. 2014; 8:12826. [PubMed: 25493908]
(22). Soskine M, Biesemans A, Moeyaert B, Cheley S, Bayley H, Maglia G. Nano Letters. 2012; 12:4895. [PubMed: 22849517]
(23). Aravind L, Koonin EV. Genome Biol. 2001; 2 RESEARCH0007.
(24). Trewick SC, Henshaw TF, Hausinger RP, Lindahl T, Sedgwick B. Nature. 2002; 419:174. [PubMed: 12226667]
(25). Chin RM, Fu X, Pai MY, Vergnes L, Hwang H, Deng G, Diep S, Lomenick B, Meli VS, Monsalve GC, Hu E, Whelan SA, Wang JX, Jung G, Solis GM, Fazlollahi F, Kaweeteerawat C, Quach A, Nili M, Krall AS, Godwin HA, Chang HR, Faull KF, Guo F, Jiang M, Trauger SA, Saghatelian A, Braas D, Christofk HR, Clarke CF, Teitell MA, Petrascheck M, Reue K, Jung ME, Frand AR, Huang J. Nature. 2014; 510:397. [PubMed: 24828042]
(26). Rodriguez-Gallego E, Guirro M, Riera-Borrull M, Hernandez-Aguilera A, Marine-Casado R, Fernandez-Arroyo S, Beltran-Debon R, Sabench F, Hernandez M, Del Castillo D, Menendez JA, Camps J, Ras R, Arola L, Joven J. International journal of obesity. 2014
(27). Nikolaidou T, Mamas M, Oceandy D, Neyses L. Heart. 2010; 96:e14.
(28). Peti-Peterdi, J. Google Patents. 2014.
(29). Bleijlevens B, Shivarattan T, Flashman E, Yang Y, Simpson PJ, Koivisto P, Sedgwick B, Schofield CJ, Matthews SJ. EMBO reports. 2008; 9:872. [PubMed: 18617893]
(30). Bleijlevens B, Shivarattan T, van den Boom KS, de Haan A, van der Zwan G, Simpson PJ, Matthews SJ. Biochemistry. 2012; 51:3334. [PubMed: 22443471]
(31). Ergel B, Gill ML, Brown L, Yu B, Palmer AG 3rd, Hunt JF. The Journal of biological chemistry. 2014; 289:29584. [PubMed: 25043760]
(32). Ogasawara Y, Funakoshi M, Ishii K. Biological & pharmaceutical bulletin. 2009; 32:1819. [PubMed: 19881290]
(33). Ludwig A, Bauer S, Benz R, Bergmann B, Goebel W. Molecular Microbiology. 1999; 31:557. [PubMed: 10027972]
(34). Wendell D, Jing P, Geng J, Subramaniam V, Lee TJ, Montemagno C, Guo P. Nature nanotechnology. 2009; 4:765.
(35). Gilbert RJ, Jimenez JL, Chen S, Tickle IJ, Rossjohn J, Parker M, Andrew PW, Saibil HR. Cell. 1999; 97:647. [PubMed: 10367893]

Europe PMC Funders Author Manuscripts

Europe PMC Funders Author Manuscripts

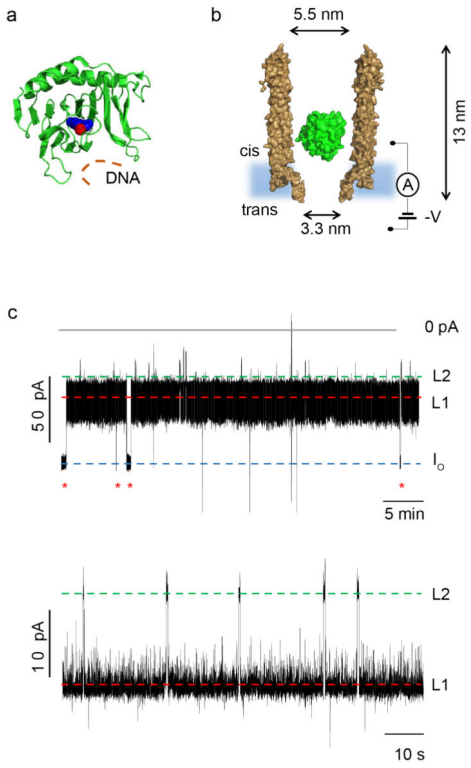

Figure 1.

Internalization of AlkB-Fe^{++} into ClyA-AS. **a**, Cartoon representation of *E. coli* AlkB (green) containing a metal ion (Co^{2+}, red sphere) and binding to the cofactor (2-OG, blue spheres). The DNA binding site is depicted by an orange line. PDB_ID 3KHB. **b**, Representation of a single AlkB-Fe^{++} enzyme (green) confined in a ClyA-AS nanopore (brown, shown as cross-section) embedded in a planar lipid bilayer (light blue) under a negative applied potential. The dimensions of the pore consider the Van der Waals radii of the atoms. **c,** Top: Typical current blockades provoked by AlkB-Fe^{++} molecules (~4 nM, *cis*) entering a ClyA-AS nanopore at −60 mV. The open pore current (I_O) is represented by a blue dashed line, while Level 1 and Level 2 are shown by red and green dashed lines, respectively. The red asterisks represent the restoration of I_O upon the exiting of AlkB-Fe^{++} from the pore. Bottom: Detail of a single AlkB-Fe^{++} blockade, showing Level 1 (red) and Level 2 (green) current levels. The current traces were collected by applying a Bessel-low pass filter with a 2 kHz cut-off and sampled at 10 kHz. An additional Bessel 8-pole filter with 50 Hz cut-off was digitally applied to the trace shown in **c,** bottom. All recordings were carried out in 150 mM NaCl, 15 mM Tris HCl pH 8.0, at 28°C, and the AlkB was added to the *cis* compartment.

Europe PMC Funders Author Manuscripts

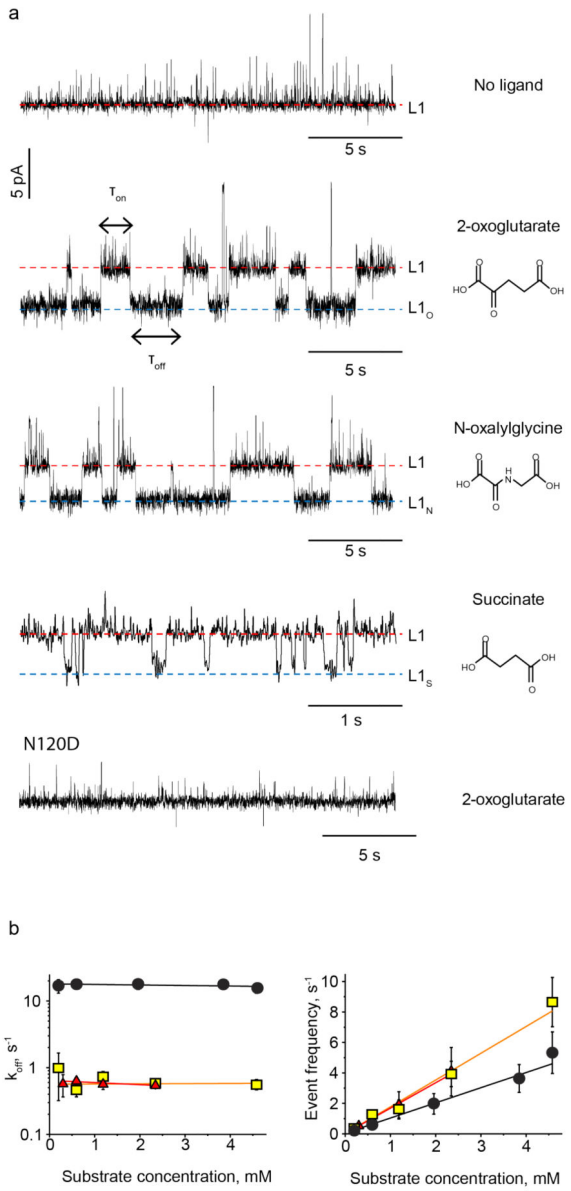

Figure 2.

Binding of ligands to AlkB-Fe^{++} confined inside ClyA-AS. **a,** Typical ligand-induced blockades to individual AlkB-Fe^{++} enzymes confined inside ClyA-AS at −60 mV. The ligand used is shown on the right of the trace. The bound Level 1 current levels ($L1_O$, $L1_N$, $L1_S$) are represented by the blue dashed lines. The substrate concentration was 0.6 mM for 2-OG, 0.6 mM for N-OG and 2 mM for SUC binding to wild type AlkB-Fe^{++}, and 7.2 mM for 2-OG binding to N120D-AlkB-Fe^{++}. **b,** Left: Dissociation rate constants (k_{off}) as a function of the ligand concentration at −60 mV. Right: Event frequency ($1/\tau_{on}$) as a function of the ligand concentration at −60 mV. 2-OG is shown in yellow squares, SUC in black circles and N-OG in red triangles. All current traces were collected by applying a Bessel-low pass filter with a 2 kHz cut-off and sampled at 10 kHz. An additional Bessel 8-pole filter with 50 Hz cut-off was digitally applied to the current traces. All recordings were carried out

in 150 mM NaCl, 15 mM Tris HCl pH 8.0, at 28°C, and the ligands were added to the *cis* compartment. Errors are given as standard deviations.

Europe PMC Funders Author Manuscripts

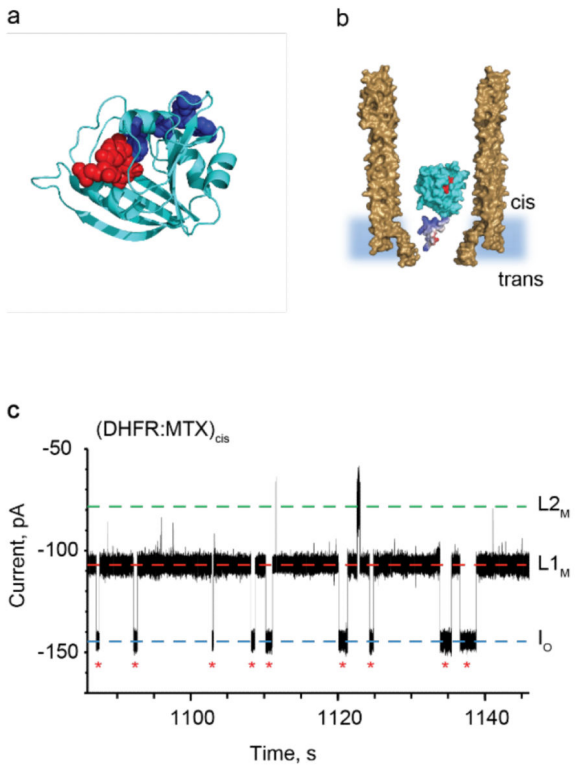

Figure 3.

DHFR as a protein adaptor. **a,** Cartoon representation of *E. coli* DHFR (cyan) with bound methotrexate (MTX, red spheres) and NADPH (blue spheres), PDB_ID 1RH3. **b**, Representation of a single $DHFR_{tag}$ enzyme (cyan) in complex with MTX (red) confined in a ClyA-AS nanopore (brown, shown as cross-section) embedded in a planar lipid bilayer (light blue) under a negative applied potential. The positively charged polypeptide tag added at the C-terminus of DHFR is shown in blue. **c,** Typical current blockades provoked by the capture of $DHFR_{tag}$:MTX complexes (20 nM $DHFR_{tag}$, 400 nM MTX, *cis*) by the ClyA-AS nanopore at −90 mV. The open pore current (I_O) is represented by a blue dashed line, while $L1_M$ and $L2_M$ are shown by red and green dashed lines, respectively. Red asterisks represent restoration of I_O upon the exiting of $DHFR_{tag}$:MTX from the pore. The current traces were collected in 150 mM NaCl, 15 mM Tris HCl pH 7.5, at 28°C by applying a Bessel-low pass filter with a 2 kHz cut-off and sampled at 10 kHz.

Europe PMC Funders Author Manuscripts

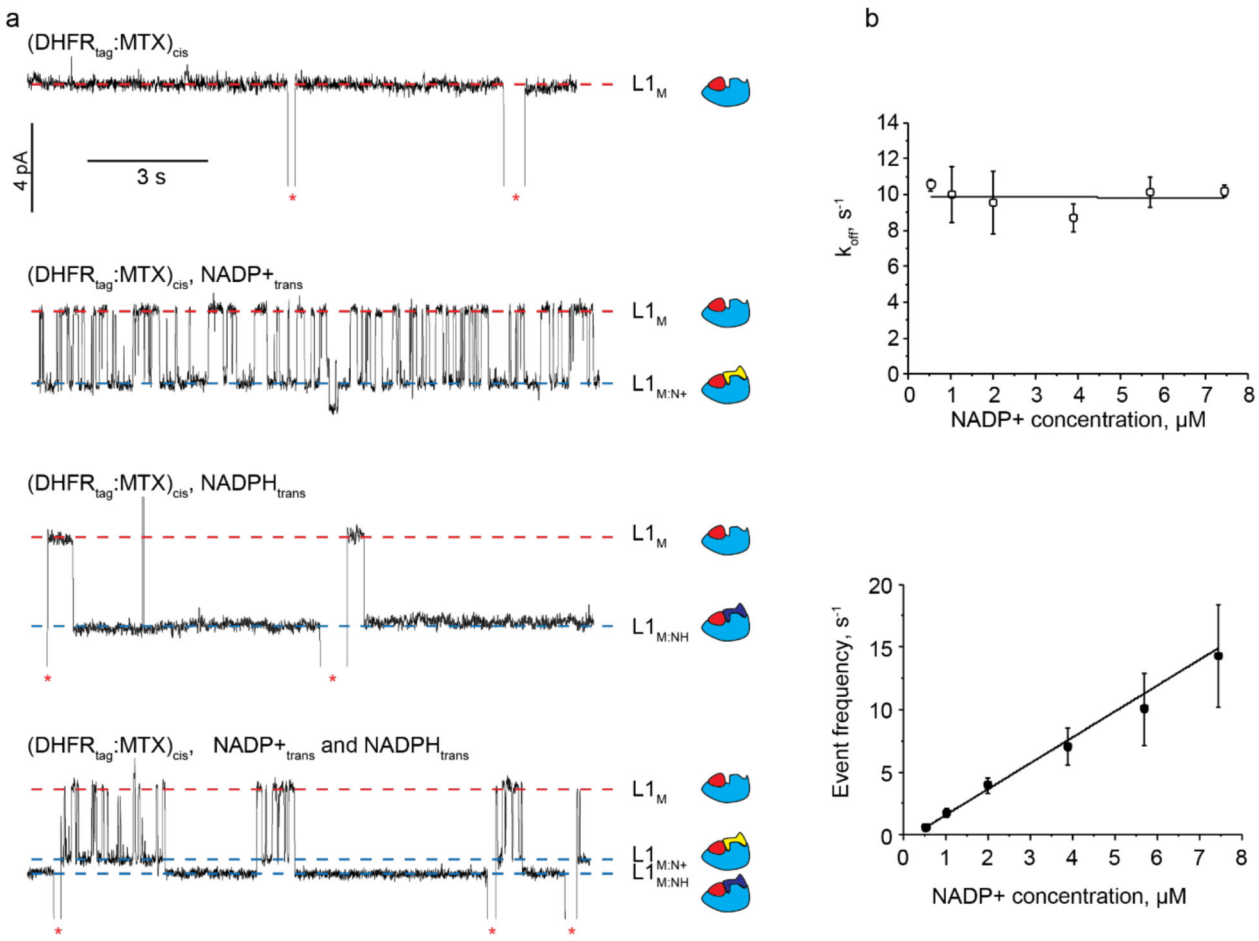

Figure 4.

Ligands binding to DHFR$_{tag}$. **a**, Ligand-induced current enhancements to individual DHFR$_{tag}$:MTX blockades at −90 mV. NADP$^+$ and NADPH are added to the *trans* compartment after addition of 20 nM DHFR$_{tag}$ and 400 nM MTX to the *cis* compartment. From top to bottom: no ligand; 5.7 μM of NADP+; 0.7 μM of NADPH; 7.4 μM of NADP+ together with 0.7 μM of NADPH. Free and bound Level 1 are shown by red and blue dashed lines, respectively. Red asterisks represent restoration of I_O upon the exit of DHFR$_{tag}$:MTX from the pore. On the right of the current traces is the schematic representation of the interaction of DHFR$_{tag}$ (cyan) with MTX (red), NADP+ (yellow) or NADPH (blue). **b,** Top: Dissociation rate constants (k_{off}) as a function of the NADP+ concentration added to the *trans* compartment at −90 mV. Bottom: Event frequency ($1/\tau_{on}$) as a function of the NADP+ concentration added to the *trans* compartment at −90 mV. Errors are shown as standard deviations. All current traces were collected by applying a Bessel-low pass filter with a 2 kHz cut-off and sampled at 10 kHz. An additional Bessel 8-pole filter with 50 Hz cut-off was digitally applied to the traces shown in **a**. All recordings were carried out in 150 mM NaCl, 15 mM Tris HCl pH 7.5, at 28°C.

Europe PMC Funders Author Manuscripts